

Photoionization microscopy of Rydberg hydrogen atom in a time-dependent electric field

DE-HUA WANG*, FEI DING

School of Physics and Optoelectronic Engineering, Ludong University, Yantai 264025, China

The photoionization microscopy of the Rydberg hydrogen atom in a time-dependent gradient electric field is investigated for the first time based on the semiclassical open orbit theory. Oscillatory pattern appears in the spatial distributions of electron probability density, which is caused by the interference between different electron trajectories that reach the detector. Compared with the photoionization in the uniform electric field, the time-dependent electric field restricts the electron motion in the plane perpendicular to the electric field and causes the number of the electron trajectories arrive at the detector plane increase significantly. Our calculation results suggest even at a macroscopic distance from the photoionization source, which is typical for an actual photoionization microscopy experiment, the interference pattern in the electron probability density still can be seen clearly. Therefore, we make predictions that our work should serve as a guide to future photoionization microscopy experiment in the time-dependent electric fields.

(Received April 2, 2018; accepted November 29, 2018)

Keywords: Photoionization microscopy, Time-dependent electric field, Semiclassical open orbit theory

1. Introduction

Imaging probability density of wave function of atoms or ions has attracted wide attention for several decades. In 1980s, Demkov and Kondratovich et al put forward the theory of the photodetachment microscopy [1-3]. In the early studies, photoelectron imaging technique could visualize only the classical envelope of the wave function. Until 1996, the direct observation of the oscillatory structure of a wave function became possible using the photodetachment microscope [4]. Blondel *et al.* firstly observed the photodetachment microscopy interference patterns of Br^- in an electric field [4]. Subsequently, they studied the photodetachment of O^- in the electric field [5]. Experimental observations of spatial interference of the electron probability density in the electric field allow very precise determination of electron affinities in the negative ions [6-8]. Later, this theory has been extended to study the photoionization of the neutral atoms in the external fields, which is called photoionization microscopy [9-11]. Photoionization adds additional features compared to photodetachment. In the photodetachment of negative ions in the electric field, only two detached electron trajectories can arrive at the detector position and the observed

oscillatory structures can be seen as a consequence of the interference between these two electron trajectories[12]. In the case of photoionization, the ionized electron trajectory becomes complex. Because of the combination of the electrostatic Coulomb potential plus the electric field potential, the electron trajectories are no longer parabolic [13-15]. At a given point on the detector plane, an infinite number of electron trajectories can arrive. The whole electron trajectories can be divided into two types: one kind electron trajectory is called the direct trajectory, which hits the detector directly without further significant interaction with the ion. The other kind is called the indirect trajectory, which encircles the nucleus for one or more orbital periods before it reaches the detector. In the calculation of the electron density probability, one has to consider the interference among an infinite number of classical trajectories. Therefore, the two-dimensional electron probability density measurements are predicted to show a considerably more complex structure. In 2002, Nicole et al. reported that they have observed a geometrical interference pattern when photoelectrons ejected in the threshold photoionization of xenon were detected in a velocity-map imaging apparatus [13]. In 2013 and 2016, Cohen et al carried out the photoionization

experiment for Rydberg lithium atom in the presence of a static electric field, and presented the photoionization wave function microscopy images [16-17]. At the same time, Stodolna et al investigated the photoionization microscopy of the hydrogen atom in an electric field and observed the nodal structure of Stark states [18-19]. The electron spatial distributions measured by their microscopy provide a validation of theoretical predictions that have been made over the last three decades [1]. In the theoretical aspect, Robicheaux and Shaw used the wave-packet dynamics method to study the photoionization of rubidium atom in a static electric field [20]. Later, a semiclassical description of photoionization microscopy was presented by Bordas et al. [21]. However, their semiclassical theory is incomplete, since they did not include the Maslov indices and did not correct the singularities appeared in the semiclassical approximation. Zhao et al amended the above defects and put forward a semiclassical open-orbit theory to describe the photoionization of hydrogen atom in the electric field [22]. The photoionization microscopy images they obtained were in agreement with those from the quantum-mechanical calculations [23], which confirmed the validity of the semiclassical open-orbit theory. Ever since then, the semiclassical open-orbit theory has been widely applied by many researchers. For example, Wang et al. have used this theory to study the photoionization of hydrogen atom in parallel electric and magnetic fields [24]. Our group has studied photoionization microscopy of hydrogen atom in a magnetic field [25]. Very recently, Liu et al developed this theory to study the photoionization microscopy on nonhydrogen atoms in the presence of a uniform electric field [26]. In these previous studies, the researchers all studied photoionization of Rydberg atom in the static electric or magnetic field. As for the photoionization of Rydberg atom in the time-dependent external fields, the reports are relatively few. In 1997, Spellmeyer et al. reported the results of an experimental and theoretical investigation of the recurrence spectra of Rydberg atom in a static electric field plus a weak oscillating electric field [27]. A detailed analysis of the recurrence spectra of Rydberg atom in the time-dependent oscillating electric field has been given by Haggerty and Delos using the semiclassical closed orbit theory [28].

Recently, Li et al studied the wave function for time-dependent harmonically confined electrons in a time-dependent electric field [29]. However, for the photoionization microscopy of Rydberg atom in the time-dependent external fields, no reports have been given to date. In this paper, we study the photoionization microscopy of Rydberg hydrogen atom in a time-dependent gradient electric field on the basis of the semiclassical open orbit theory. The distribution of the ionized electron probability density on the detector plane perpendicular to the electric field is calculated. Replacing static electric field with time-dependent electric field adds new interesting physics. If the electric field is varied with time, the electron trajectories become much more complicated. An infinite number of electron trajectories will reach the detector plane, leading to an extremely complicated interference patterns on the detector. In addition, the photoionization microscopy interference pattern at the detector depends sensitively on the electric field gradient, the electron energy and the position of the detector plane. Even at a macroscopic distance from the detector to the ion source, the photoionization microscopy interference pattern can be seen clearly. Therefore, our work provides some references for the photoionization microscopy experiment in the time-dependent electric field. Atomic unit is used unless specified otherwise.

2. Theory and quantitative formula

Fig. 1 shows the physical picture of the photoionization of hydrogen atom in a time-dependent electric field. Suppose the time-dependent gradient electric field lies along the z direction: $F = F_0 + \alpha t$, where F_0 is the background uniform electric field, α is the electric field gradient, $\alpha > 0$ [30]. A detector plane is perpendicularly to the $-z$ axis. The distance from the detector plane to the hydrogen nucleus is z_0 . The photoionization process of hydrogen atom in the external electric field can be regarded as a two step process: in the first step, after a beam of laser light shines on the hydrogen atom, the electron will absorb a photon and jump to a high energy state; in the second step, the ionized electron waves propagate outward from the nucleus along

classical trajectories. Due to the combined interaction of the Coulomb force and the electric field force, some electron trajectories may escape from the atom, and arrive at a detector plane perpendicular to the electric field. Following Zhao and Delos' description [22], these electron trajectories are called open orbits. Whenever two or more than two electron trajectories reach the same point on the detector plane, the constructive or destructive interference between the corresponding electron waves lead to an observable microscopy pattern on the detector, as shown in Fig. 1.

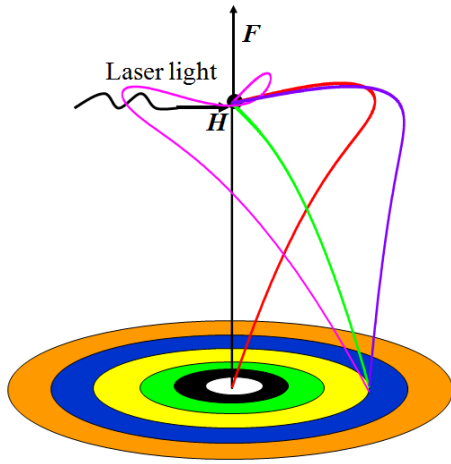


Fig. 1. (Color online) Physical picture description of the photoionization of hydrogen atom in a time-dependent electric field. The detector plane is perpendicular to the electric field. At a same point on the detector plane, several electron trajectories can arrive, leading to a set of concentric interference fringes

The Hamiltonian of the ionized electron in the Coulomb plus the time-dependent gradient electric field is (in cylindrical coordinates):

$$H = \frac{1}{2}(p_\rho^2 + p_z^2) - \frac{1}{\sqrt{\rho^2 + z^2}} + (F_0 + \alpha t)z \equiv E, \quad (1)$$

where the z component of angular momentum is chosen to be zero.

Using the scaled variables: $\tilde{\rho} = \rho F_0^{1/2}$, $\tilde{z} = z F_0^{1/2}$,

$$\tilde{\alpha} = \alpha F_0^{-1}, \quad \tilde{p}_\rho = p_\rho F_0^{-1/4}, \quad \tilde{p}_z = p_z F_0^{-1/4} \quad \text{and}$$

$\tilde{\varepsilon} = E F_0^{-1/2}$, we get the scaled Hamiltonian (the tilde “~” has been omitted):

$$H = \frac{1}{2}(p_\rho^2 + p_z^2) - \frac{1}{\sqrt{\rho^2 + z^2}} + (1 + \alpha t)z = \varepsilon. \quad (2)$$

In order to remove the Coulomb singularity at the origin in the above equation, we introduce parabolic coordinates (u, v) and their conjugate momenta (p_u, p_v) defined by[31]:

$$u = \sqrt{r + z}, \quad v = \sqrt{r - z}, \quad (3)$$

$$p_u = v p_\rho + u p_z, \quad p_v = u p_\rho - v p_z \quad (4)$$

Here $r = \sqrt{\rho^2 + z^2} = (u^2 + v^2)/2$. A new scaled

time variable τ is given by $d\tau/dt = 1/(u^2 + v^2)$.

Then we get an effective Hamiltonian

$$h = (u^2 + v^2)(H - \varepsilon):$$

$$h = \frac{1}{2}(p_u^2 + p_v^2) - \varepsilon(u^2 + v^2) + \frac{1}{2}(1 + \alpha t)(u^4 - v^4) - 2 \quad (5)$$

Suppose the ionized electron is emitted from the origin with the outgoing angle θ_i ,

$$\theta_i = \tan^{-1}(\rho/z) = 2 \tan^{-1}(v/u), \quad \text{which is the angle}$$

between the initial velocity of the electron and the electric field. By setting $h=0$ and integrating the Hamiltonian motion equations, we can obtain the electron trajectories that have arrived at the detector point. In Fig. 2, we plot some electron trajectories that have arrived at the same detector point $\rho = 1.0, z = -4.0$.

Fig. 2 (a) shows the electron trajectories with a large initial outgoing angle $\theta_i = 2.62$ (rad). Under this condition, the electron is emitted in downward direction, the initial velocity along the $-z$ axis is large, the gradient electric field force plays the dominate role. Then after a short period of time, it reaches the detector without rotating in the ρ - z plane. We call this kind of trajectory the direct trajectory. Fig. 2(b) shows the electron trajectories with a small outgoing angle $\theta_i = 0.22$ (rad). Both the Coulomb force and the electric field force will affect the electron motion, which causes the electron trajectory rotate in the ρ - z plane. After the electron trajectory encircles the

nucleus once, it finally hits the detector. This kind of orbit is called the indirect trajectory. As we further decrease the outgoing angle θ_i , the electron trajectory becomes very

complex. It will encircle the nucleus several times before it reaches the detector, as shown in Figs. 2(c-f).

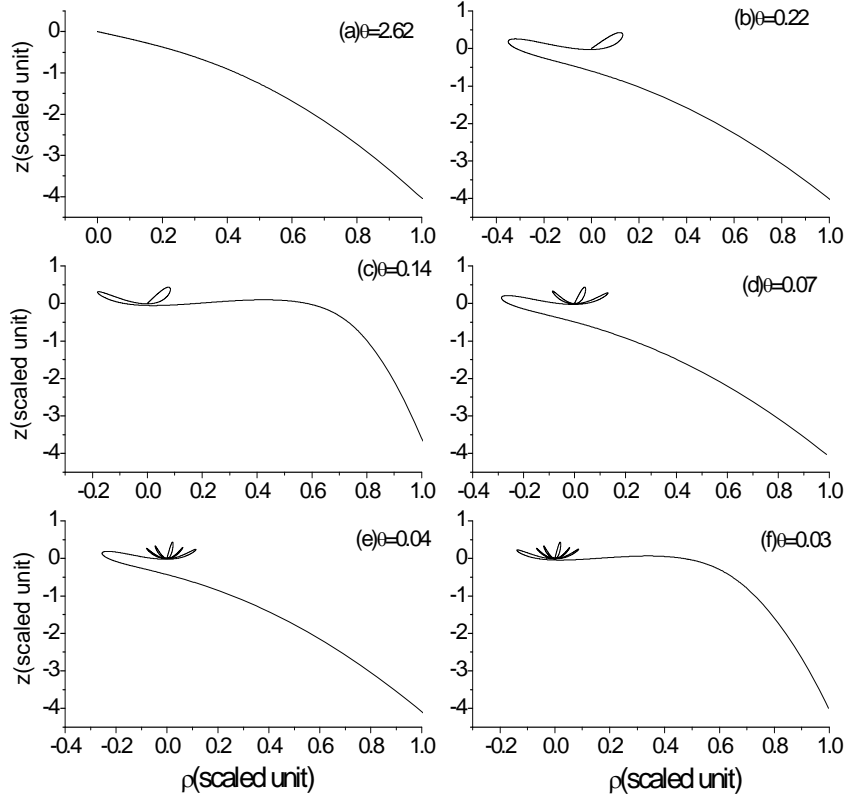


Fig. 2. Some classical electron trajectories in the time-dependent gradient electric field arriving at the same point ($\rho = 1.0, z = -4.0$) on the detector. The scaled energy $\mathcal{E} = -0.1$, the scaled electric field gradient $\mathcal{A} = 10.0$, the detector is located at $z = -4.0$ plane. The initial outgoing angle of each trajectory is given in the plot

In the following, we construct the electron wave function on the basis of the semiclassical approximation. For any point $M(\rho, z_0)$ on the detector plane, more than one electron trajectory can pass through it. Corresponding to j -th trajectory, the electron wave function is denoted by $\psi_j(\rho, z_0)$, which depends on its classical density A_j and a classical action function $S_j(\rho, z_0, E)$:

$$\psi_j(\rho, z_0) = \sqrt{A_j(\rho, z_0)} e^{i[S_j(\rho, z_0, E) - \frac{\pi}{2}\lambda_j]}, \quad (6)$$

here, the classical density A_j is given by[24]:

$$A_j(\rho, z_0) = \frac{d\theta_j}{d\rho} \sin \theta_j. \quad \text{The classical action } S_j \text{ is}$$

defined by: $S_j(\rho, z_0, E) = \int_0^{M(\rho, z_0)} \vec{p} \cdot d\vec{q}$. $\omega = F_0^{-1/4}$ is a

scaled factor. λ_j is the Maslov index, which equals to the number of extremas in the ρ direction plus the number of crossings of the z -axis. The purpose of introducing Maslov index is to correct the phase due to the failure of the semiclassical approximation.

The final wave function $\psi_f(\rho, z_0)$ at point $M(\rho, z_0)$ is obtained by summing all the electron trajectories from the ion source to the detector point:

$$\begin{aligned}\psi_f(\rho, z_0) &= \sum_{j=1}^n \psi_j(\rho, z_0) \\ &= \sum_{j=1}^n \left[\frac{d\theta_j}{d\rho} \sin \theta_j \right]^{1/2} e^{i[S_j(\rho, z_0, E)\omega - \frac{\pi}{2}\lambda_j]}\end{aligned}\quad (7)$$

The calculated radial electron probability density distribution at a given point $M(\rho, z_0)$ on the detector is:

$$\begin{aligned}P(\rho, z_0, \varphi) &= |\psi_f(\rho, z_0, \varphi)|^2 \\ &= \sum_{j=1}^n |A_j|^2 + 2 \sum_{i < j} A_i A_j \cos[S_i - S_j - \frac{\pi}{2}(\lambda_i - \lambda_j)]\end{aligned}\quad (8)$$

From the above equation, we find that the electron probability density distribution at the detector point includes two parts: the first part corresponds to the classical probability density distribution, while the second part represents the interference among different classical trajectories arriving at the detector point.

3. Results and discussions

Using Eq. (8), we can calculate the electron probability density distribution on the detector plane. Firstly, we keep the detector localized at the $z=-z_0=-4.0$ (scaled unit) plane. Based on the scaled transformation, $\tilde{z} = zF_0^{1/2}$, if we choose the background electric field strength $F_0=19\text{V/cm}$, then the distance from the ion to the detector is $z_0=3.48\mu\text{m}$. By solving the Hamiltonian motion equations (Eq.(5)), we can find out all the possible ionization electron trajectories in the time-dependent gradient electric field. It is obvious that the number of the electron trajectories depends on the evolution time of the electron in the gradient electric field. In the following calculation, we take $T_{\text{max}} = 20$ (scaled unit). For each electron trajectory arrived at the detector, we record its initial outgoing angle θ_i , the impact point ρ on the detector and the Maslov index λ_i , then we can calculate the electron probability density.

Fig. 3(a) shows a graph of the final position ρ on the detector plane versus the initial outgoing angle θ_i . The scaled energy $\varepsilon = -0.1$ and the scaled electric field

gradient $\alpha = 10$. From this figure, we find at a given point on the detector plane, multiple electron trajectories can arrive at. The whole $\rho - \theta$ curve can be separated into several different regions, which are denoted by the number 1, 2, 3, In the first region, $0.82 \leq \theta \leq \pi$, the influence of the gradient electric field is very small, the electron trajectory is similar to the hydrogen atom in a pure electric field, which likes a parabola. The electron trajectories can reach the detector directly without rotating in the ρ - z plane, which belong to the direct ones. However, in the second region, $0.25 \leq \theta < 0.82$, the influence of the gradient electric field begins to appear. The electron will encircle the nucleus once before it reaches the detector. These electron trajectories are the indirect ones. In the third region, $0.13 \leq \theta < 0.25$, the electron will encircle the nucleus twice before it reaches the detector. The electron trajectories in the other regions can be analyzed in the similar way. In Fig. 3(b), we calculate the radial electron probability density distribution on the detector plane. Oscillatory structures appear in the electron probability density, which can be considered as a consequence of the interference between different electron trajectories in the Coulomb field plus the gradient electric field. In order to show the electron probability density distribution on the detector plane clearly, we calculate the three-dimensional probability density distribution on the detector plane, which is shown in Fig. 3(c). Fig. 3(d) is the photoionization microscopy image corresponds to Fig. 3(c), which can be measured in the actual photoionization microscopy experiment. A series of bright and dark concentric interference rings appears in the electron probability density distribution. The bright rings are caused by the constructive interference of different electron trajectories, while the dark rings correspond to the destructive interference between different electron trajectories.

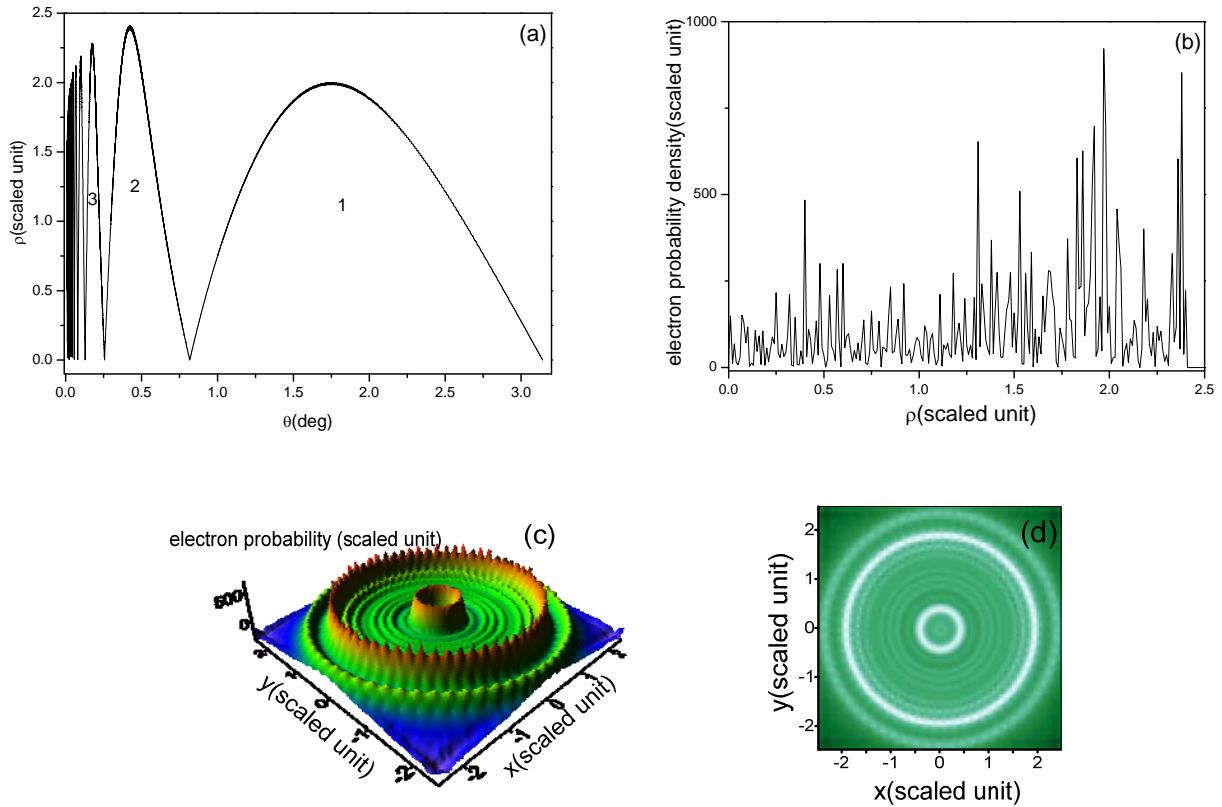


Fig. 3. The calculated photoionization microscopy of a hydrogen atom in the time-dependent gradient electric field with the scaled energy $\mathcal{E} = -0.1$, the scaled electric field gradient $\alpha = 10.0$, and the detector is located at $z = -4.0$ plane. (a) The impact position ρ at the detector plane versus the initial outgoing angle θ of the electron trajectory. (b) The two-dimensional electron probability density distribution on the detector plane. (c) The three-dimensional electron probability density distribution on the detector plane; (d) The photoionization microscopy image plot of Fig. 3(c)

In Fig. 4, we restrict the outgoing angle of the electron to different region and calculate the interference patterns in the electron probability density caused by different electron trajectories. Some typical interference patterns with prominent contributions to the electron probability density are shown in Fig. 4. Fig. 4(a) shows the electron probability density caused by the direct electron trajectories, with the outgoing angle lies in the first region $0.82 \leq \theta \leq \pi$. It is found that the oscillatory structure in the electron probability density is only limited in the region $0 \leq \rho \leq 2.0$, which plays a significant role in the inner region of the photoionization microscopy image. This kind of electron trajectories makes no contribution to the outer region $2.0 < \rho \leq 2.41$. Fig. 4(b) shows the electron probability density caused by the electron trajectories lies

in the second region, $0.25 \leq \theta < 0.82$. We can see the electron probability density distribution spreads widely, which dominates the signal in the outer region ($2.0 < \rho \leq 2.41$) of the photoionization microscopy image. Figs. 4(b-c) is the electron probability density caused by the electron trajectories lies in the third region ($0.13 \leq \theta < 0.25$) and fourth region ($0.08 \leq \theta < 0.13$), respectively. We find the influences of these electron trajectories to the electron probability density distributions are very small. Unlike the above two patterns in Fig. 4(a) and (b), they give a weak signal to the photoionization microscopy image, and only modulate the whole region in the radial distribution of the electron probability density.

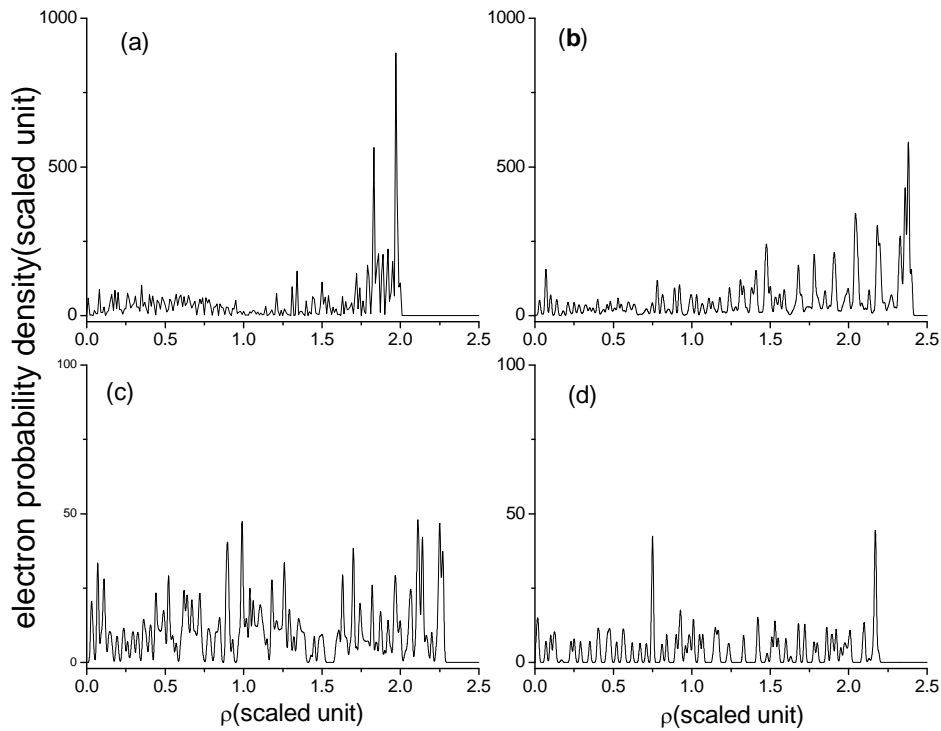


Fig. 4. The electron probability density distribution on the detector located at $z=-4.0$ plane for a hydrogen atom in the time-dependent gradient electric field, corresponding to electron trajectories belong to different regions. The scaled energy $\mathcal{E} = -0.1$ and the scaled electric field gradient $\alpha = 10.0$. (a) The electron probability density corresponds to the contribution of the direct electron trajectories, with the outgoing angle lies in the first region $0.82 \leq \theta \leq \pi$; (b)-(d) The electron probability density caused by the electron trajectories lies in the second region $0.25 \leq \theta < 0.82$, the third region $0.13 \leq \theta < 0.25$ and the fourth region $0.08 \leq \theta < 0.13$, respectively

Next, we keep the scaled energy $\mathcal{E} = -0.1$ unchanged, and study the variation of photoionization microscopy image on the detector plane with the electric field gradient. Fig. 5(a) shows the ρ - θ curve with the electric gradient $\alpha = 0$, which is similar to the photoionization of hydrogen atom in a uniform electric field [22]. A critical angle $\theta_c = 0.11$ is existed. If the ionized electron emitted at an angle larger than θ_c , it will escape the Coulomb and electric field forces and reach the detector. However, as the outgoing angle is smaller than θ_c , it will remain in the vicinity of the nucleus and cannot reach the detector within the given time. Fig. 5(b) shows the ρ - θ curve with the scaled electric gradient $\alpha = 3.0$, there still exists a critical angle θ_c , but it is smaller than the case given in Fig. 5(a), $\theta_c = 0.048$. The whole ρ - θ curve can be separated into several different regions. In the region $0.76 \leq \theta \leq \pi$, the electron trajectories can reach the detector directly without rotating in the ρ - z plane, these trajectories belong to the direct ones. However, in the region $0 \leq \theta \leq 0.76$, the electron will encircle the nucleus one or more orbital periods before it reaches the detector, these trajectories are the indirect ones. As we further increase the scaled electric field gradient, the number of the electron trajectories reaching the detector plane becomes

increased, nearly all the electron trajectories can escape the Coulomb and electric field forces and reach the detector plane within the given time. In addition, the maximum impact radius that the electron can arrive at the detector plane decreases correspondingly. For example, in Fig. 5(a), the maximum impact radius that the electron can reach is $\rho_{\max} = 4.33$. As the scaled electric field gradient increases to $\alpha = 200.0$, the maximum impact radius decreases to $\rho_{\max} = 1.37$. The reason is as follows: Based on the electromagnetic field theory, the variation of the electric field plays a role of the magnetic field, which will restrict the electron motion in the ρ - z plane. Therefore, when the gradient electric field is added to the Coulomb field, it will cause the electron oscillate more rapidly than the case of a pure electric field. The bigger the electric field gradient, the larger influence the gradient electric field will have to the electron motion. If the electric field gradient is very big, the electric field force becomes strong, which causes the maximum impact radius that the electron can reach the detector plane gets much smaller. See Figs. 5(c) – 5(f).

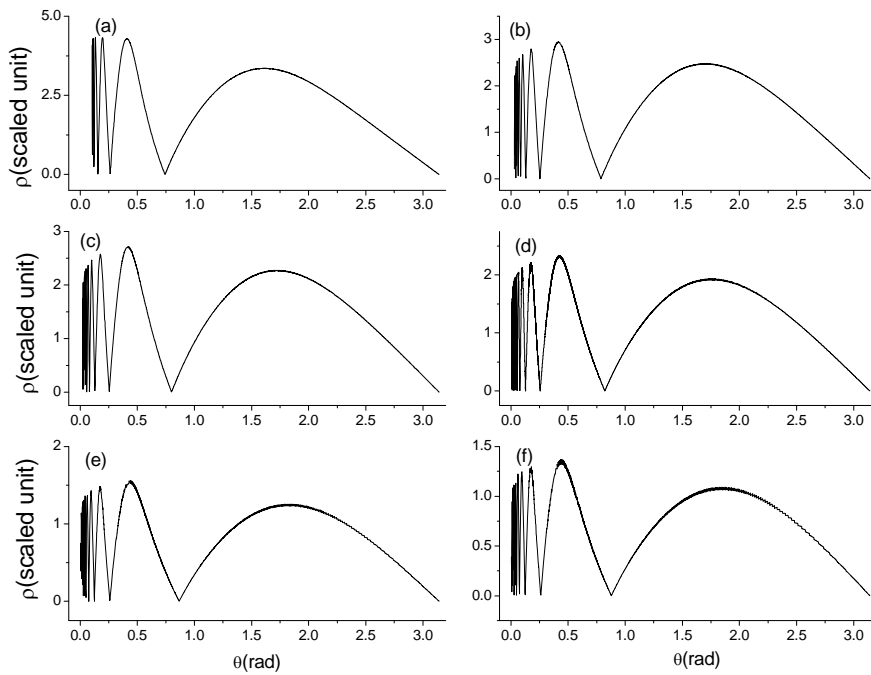


Fig. 5. Variation of the ρ - θ curve with the electric field gradient for the photoionization of Rydberg hydrogen atom. The detector is located at $z = -4.0$ plane. The scaled energy is $\varepsilon = -0.1$. The scaled electric field gradient is as follows: (a) $\alpha = 0.0$; (b) $\alpha = 3.0$; (c) $\alpha = 5.0$; (d) $\alpha = 12.0$; (e) $\alpha = 100.0$; (f) $\alpha = 200.0$

Fig. 6 shows the variation of the electron probability density distributions with the electric field gradient, the scaled energy $\varepsilon = -0.1$. In Fig. 6(a), the electric field gradient $\alpha = 0.0$, only the Coulomb force and the background uniform electric field can influence the electron motion. The maximum impact radius on the detector plane is large, and the oscillatory structure in the electron probability density distributions spreads widely. Fig. 6(b) shows the electron probability density distribution with the gradient electric field being applied, the electric field gradient $\alpha = 3.0$. The gradient electric field causes electron to oscillate perpendicular to the electric field much rapidly than the case of a pure electric field. Some of the direct electron trajectories corresponding to the case of a pure electric field are affected by the gradient electric field. The number of the

indirect electron trajectories gets increased, which makes the oscillatory structure in the electron probability density distributions becomes complicated. In addition, the gradient electric field restricts the motion of the electron in the ρ - z plane, the maximum impact radius that the electron can reach the detector plane gets decreased, which causes the oscillating region in the electron probability density becomes narrow. As we further increase the electric field gradient, the influence of the gradient electric field on the electron motion becomes significant. The maximum impact radius on the detector plane decreases, which restricts the electron probability density distribution in a small region. However, the interference effect among different electron trajectories gets stronger, which causes the oscillatory structure in the electron probability density distribution get much more complex.

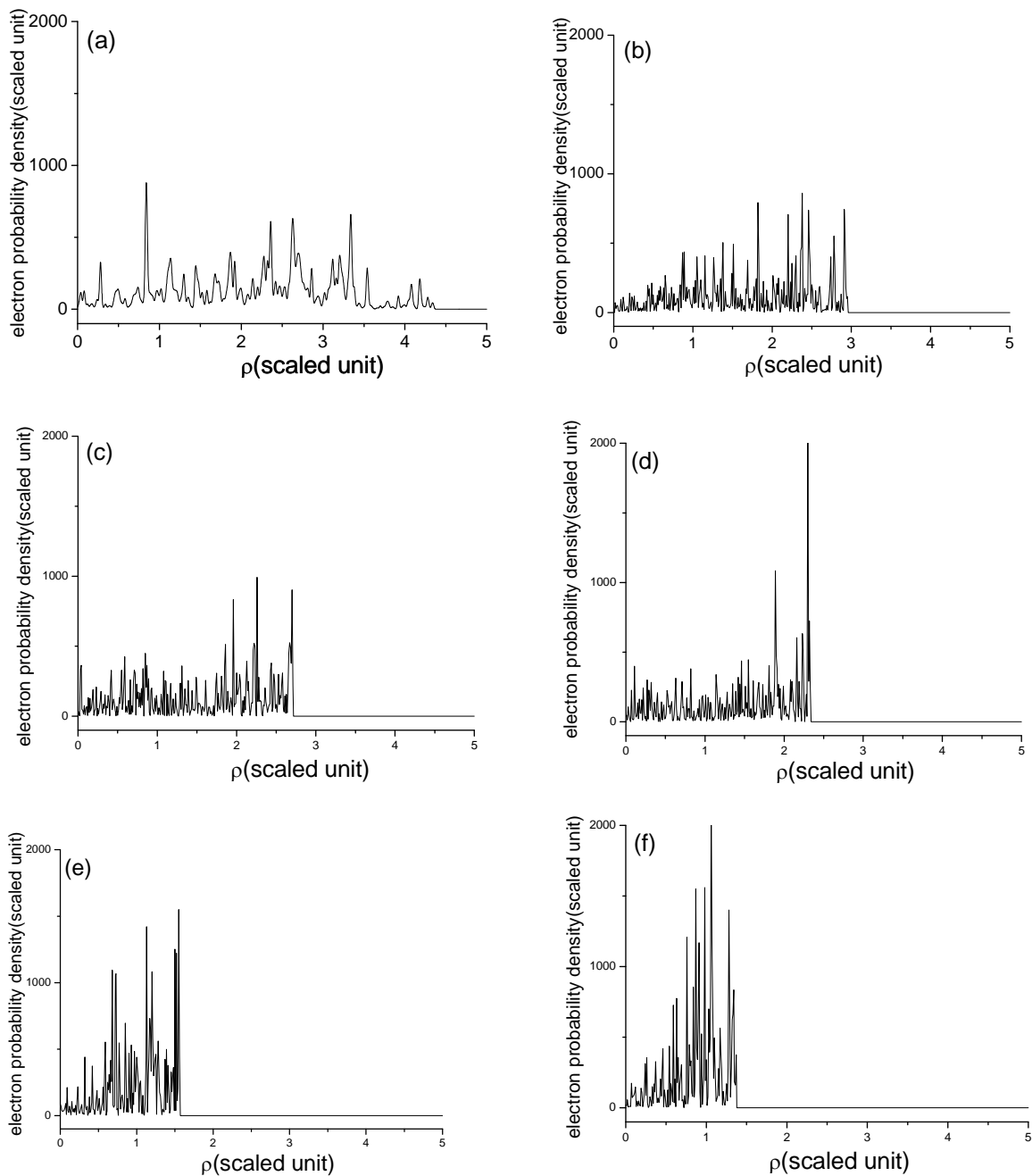


Fig. 6. Variation of the electron probability density distribution with the electric field gradient for the photoionization of Rydberg hydrogen atom. The detector is located at $z = -4.0$ plane. The scaled energy is $\varepsilon = -0.1$. The scaled electric field gradient is as follows: (a) $\alpha = 0.0$; (b) $\alpha = 3.0$; (c) $\alpha = 5.0$; (d) $\alpha = 12.0$; (e) $\alpha = 100.0$; (f) $\alpha = 200.0$

In Fig. 7, we plot the photoionization microscopy images on the detector plane correspond to Fig. 6. Fig. 7(a) is the photoionization microscopy image of the hydrogen atom in the uniform electric field. The size of the image is very large. With the increase of the electric field gradient,

the size of the photoionization microscopy image becomes decreases. As the electric field gradient is very large, $\alpha = 200$, the size of the image shown in Fig. 7(f) is extremely small.

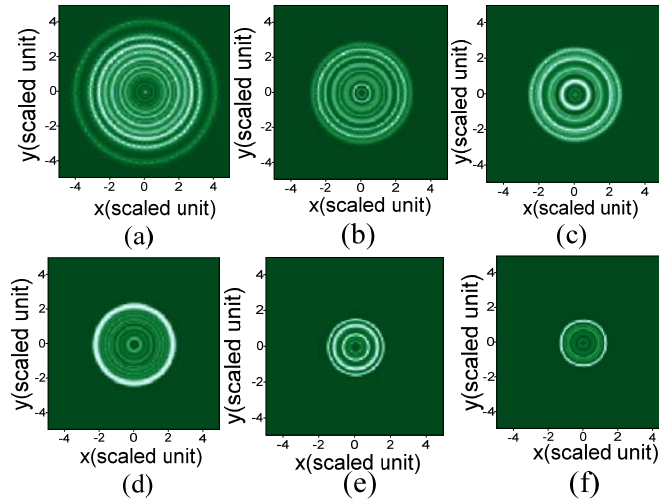


Fig. 7. Variation of the photoionization microscopy images with the electric field gradient for the photoionization of Rydberg hydrogen atom. The detector is located at $z = -4.0$ plane. The scaled energy is $\varepsilon = -0.1$. The scaled electric field gradient is as follows: (a) $\alpha = 0.0$; (b) $\alpha = 3.0$; (c) $\alpha = 5.0$; (d) $\alpha = 12.0$; (e) $\alpha = 100.0$; (f) $\alpha = 200.0$

Fig. 8 presents a series of simulations of the ρ - θ curve in the gradient electric field with $\alpha = 10$ and at a range of scaled energy between $\varepsilon = 0$ and $\varepsilon = -2.0$. Fig. 8(a) shows the ρ - θ curve with the scaled energy $\varepsilon = 0.0$. The whole region in the ρ - θ curve is dominated by the direct trajectories, which lies in the region $0.79 \leq \theta \leq \pi$. The other electron trajectories with the outgoing angle $0 < \theta < 0.79$ are the indirect ones.

As we decrease the scaled energy, the range of the

outgoing angle for the direct trajectory becomes narrow, and the number of the indirect electron trajectories can reach the detector plane get increased. As the scaled energy decreases to $\varepsilon = -2.0$, we find the ρ - θ curve on the detector plane becomes much more complex and exhibits some certain self-similarity fractal structure, which is similar to the photoionization of hydrogen atom in parallel electric and magnetic fields.

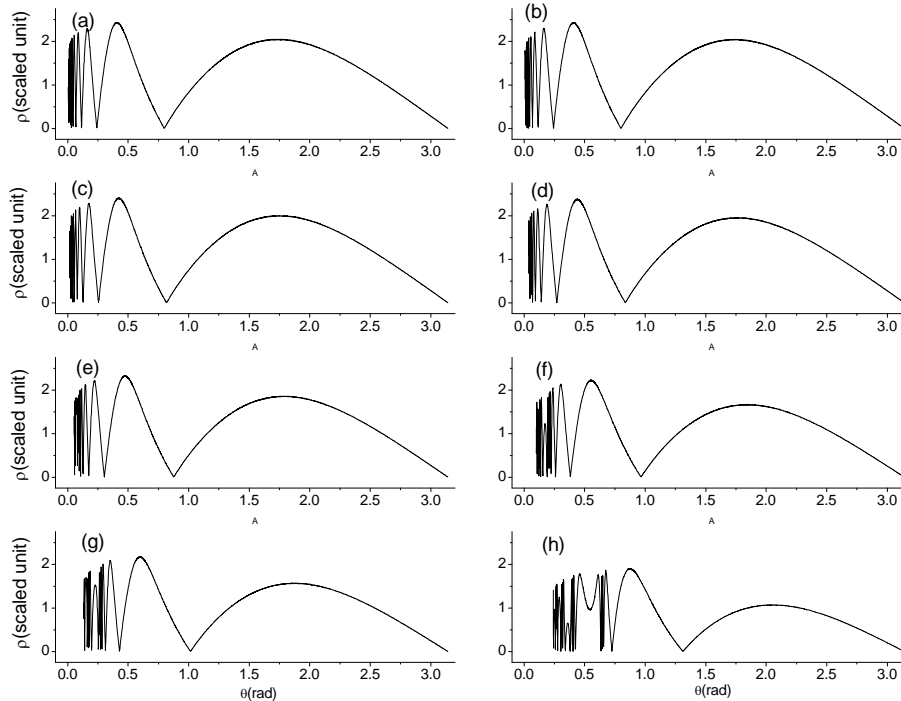


Fig. 8. Variation of the ρ - θ curve with the scaled electric field for the photoionization of Rydberg hydrogen atom. The detector is located at $z = -4.0$ plane. The scaled electric field gradient $\alpha = 10.0$. The scaled energy is as follows: (a) $\varepsilon = 0$; (b) $\varepsilon = -0.01$; (c) $\varepsilon = -0.2$; (d) $\varepsilon = -0.4$; (e) $\varepsilon = -0.6$; (f) $\varepsilon = -0.8$; (g) $\varepsilon = -1.0$; (h) $\varepsilon = -2.0$

In Fig. 9, we show a series of radial electron probability density distribution in the gradient electric field with $\alpha = 10$, the scaled energy is varied between $\varepsilon = 0$ and $\varepsilon = -2.0$. It is found that when $\varepsilon = 0$, the oscillatory structure caused by the direct electron trajectories play the dominate role, corresponding to direct ionization. In addition, the oscillating amplitude in the electric probability density distribution is relatively small. With the decrease of the scaled energy, the oscillating region in the electron probability density distribution gets decreased, but the oscillating amplitude increases significantly.

At the scaled energy $\varepsilon = -2.0$, the electric probability density distribution becomes much more complicated. For the impact radius $0 < \rho < 1.08$, the direct electron trajectories have some contribution to the oscillations in the electron probability density. However, in the other regions, the oscillatory pattern arises predominately from the interference between different indirect electron trajectories corresponding to the indirect ionization.

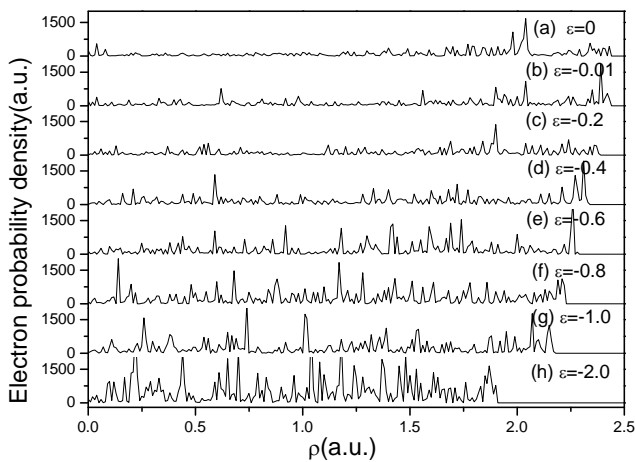


Fig. 9. Variation of the electron probability density distribution on the detector plane with the scaled electric field gradient for the photoionization of Rydberg hydrogen atom. The detector is located at $z = -4.0$ plane. The scaled electric field gradient $\alpha = 10.0$. The scaled energy is given in the plot

In the above calculations, the detector plane is localized at the $z = -z_0 = -4.0$ (scaled unit) plane. After

removing the scaled transformation, the distance from the ion to the detector is equivalent to $z_0 = 3.48 \mu\text{m}$. This distance is still too close to the ion to be relevant in the actual photoionization microscopy experiments, in order for the result to be experimentally measurable, we fix the detector plane at $z = -z_0 = -4000.0$ (scaled unit) plane. This distance from the ion to the detector equals to $z_0 = 3.48 \text{mm}$ before the scaled transformation. The evolution time of the ionization electron in the gradient electric field is increased to $T_{\text{max}} = 50$ (scaled unit). Then we calculate

the electron probability density distribution on the detector plane. We choose the scaled energy $\varepsilon = -0.1$ and the electric field gradient $\alpha = 10$. Fig. 10(a) shows the radial electric probability density as a function of the impact radius ρ on the detector plane. Oscillatory structures appear in the electric probability density, and the oscillating region is relatively large. The whole oscillating region can be divided into two parts. In the first part, $0 < \rho < 55.17$, the oscillations in the electron probability density are caused by the interference between the direct and indirect electron trajectories. However, in the outer region, the oscillatory pattern is mainly caused by the indirect electron trajectories. In order to show the electron probability density distribution on the detector plane clearly, we further plot the three-dimensional image pattern of the electron probability density on the detector plane, which is shown in Fig. 10(b). A series of interference rings appear in the electron probability density distribution, which can be measured on the position-sensitive detector in the actual photoionization microscopy experiment. Although this distance from the ion to the detector plane reaches the macroscopic dimension, we still observe a series of clear interference fringes in the photoionization microscopy image. Therefore, this work can guide the photoionization microscopy experiment in the time-dependent electric field.

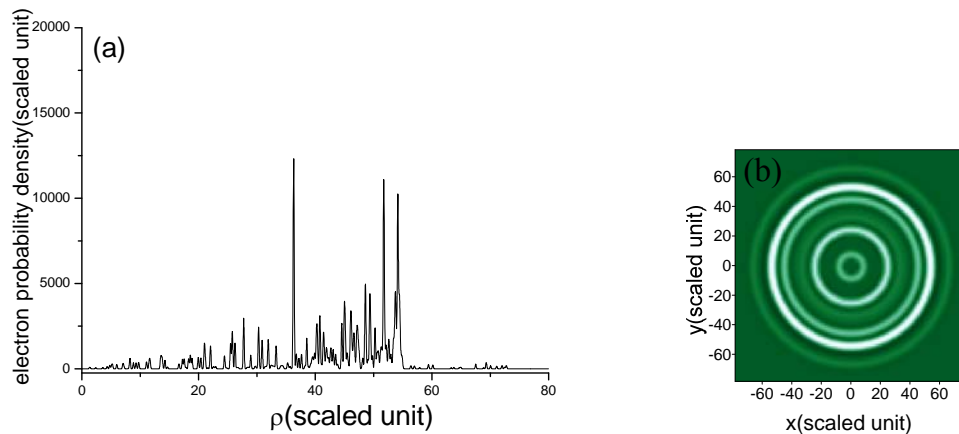


Fig. 10. The photoionization microscopy of a hydrogen atom in the time-dependent gradient electric field with the detector located at $z=-z_0=-4000.0$ (scaled unit) plane. The scaled energy $\mathcal{E}=-0.1$, and the scaled electric field gradient $\mathcal{A}=10.0$. (a) The two-dimensional electron probability density distribution on the detector plane. (b) The photoionization microscopy image on the detector plane

4. Conclusions

In conclusion, we have investigated the photoionization microscopy of Rydberg hydrogen atom in a time-dependent electric field by calculation of the electron probability density distribution on a detector plane. For the calculation of the electron probability density, we have used the semiclassical approximation to construct the wave function, the amplitude and classical action corresponding to each wave function are calculated by numerical integration of the classical motion equations of the ionized electron. We have investigated the spatial interference structures in the electron probability density contributed by different types of electron trajectories. It is found that the oscillatory structures in the electron probability density distribution depend on the electric field gradient, the scaled energy and the position of the detector sensitively. Even as the detector plane located at a macroscopic distance from the photoionization source, the photoionization microscopy interference patterns can be observed clearly. Therefore, our results provide some references for the photoionization microscopy experiment of the Rydberg atoms in a time-dependent electric field. In this work, we have carried out the specific calculations for the Rydberg hydrogen atom, since this atom is the simplest, which only has one electron outside the nucleus, its theoretical analysis is relatively simple. However, the method used in this work is universal, which can be easily extended to multi-electron atom, such as helium atom, lithium atom, etc.

Acknowledgements

This work is supported by the National Natural

Science Foundation of China under grant No. 11374133, and Taishan scholars project of Shandong province (ts2015110055).

References

- [1] Yu. N. Demkov, V. D. Kondratovich, V. N. Ostrovsky, *JETP Lett.* **34**, 425 (1981).
- [2] V. D. Kondratovich, V. N. Ostrovsky, *J. Phys. B* **17**, 1981 (1984).
- [3] V. D. Kondratovich, V. N. Ostrovsky, *J. Phys. B* **17**, 2011 (1984).
- [4] C. Blondel, C. Delsart, F. Dulieu, *Phys. Rev. Lett.* **77**, 3755 (1996).
- [5] C. Blondel, C. Delsart, F. Dulieu, C. Valli, *Eur. Phys. J. D* **5**, 207 (1997).
- [6] C. Valli, C. Blondel, C. Delsart, *Phys. Rev. A* **59**, 3809 (1999).
- [7] C. Blondel, C. Delsart, F. Goldfarb, *J. Phys. B* **34**, L281 (2001).
- [8] C. Blondel, W. Chaibi, C. Delsart, C. Drag, F. Goldfarb, S. Kroger, *Eur. Phys. J. D.* **33**, 335 (2005).
- [9] C. Nicole, H. L. Offerhaus, M. J. J. Vrakking, F. Lepine, C. Bordas, *Phys. Rev. Lett.* **88**, 133001 (2002).
- [10] Oliver L. A. Monti, Thomas A. Baker, David J. Nesbitt, *J. Chem. Phys.* **125**, 154709 (2006).
- [11] F. Lepine, C. Bordas, C. Nicole, M. J. J. Vrakking, *Phys. Rev. A* **70**, 033417 (2004).
- [12] M. L. Du, *Phys. Rev. A* **40**, 4983 (1989).
- [13] C. Nicole, H. L. Offerhaus, M. J. J. Vrakking, F. Lepine, C. Bordas, *Phys. Rev. Lett.* **88**, 133001 (2002).

- [14] T. Barillot, R. Brédy, G. Celep, S. Cohenmore, *J. Chem. Phys.* **147**, 013929 (2017).
- [15] L. B. Zhao, J. B. Delos, *Phys. Rev. A* **81**, 053417 (2010).
- [16] S. Cohen, M. M. Harb, A. Ollagnier, F. Robicheaux, M. J. J. Vrakking, T. Barillot, F. Lépine, C. Bordas, *Phys. Rev. Lett.* **110**, 183001 (2013).
- [17] S. Cohen, M. M. Harb, A. Ollagnier, F. Robicheaux, M. J. J. Vrakking, T. Barillot, F. Lépine, C. Bordas, *Phys. Rev. A* **94**, 013414 (2016).
- [18] A. S. Stodolna, A. Rouzée, F. Lépine, S. Cohen, F. Robicheaux, A. Gijsbertsen, J. H. Jungmann, C. Bordas, M. J. J. Vrakking, *Phys. Rev. Lett.* **110**, 213001 (2013).
- [19] A. S. Stodolna, F. Lépine, T. Bergeman, F. Robicheaux, A. Gijsbertsen, J. H. Jungmann, C. Bordas, M. J. J. Vrakking, *Phys. Rev. Lett.* **113**, 103002 (2014).
- [20] F. Robicheaux, J. Shaw, *Phys. Rev. A* **56**, 278 (1997).
- [21] Ch. Bordas, F. Lépine, C. Nicole, M. J. J. Vrakking, *Phys. Rev. A* **68**, 012709 (2003).
- [22] L. B. Zhao, J. B. Delos, *Phys. Rev. A* **81**, 053417 (2010).
- [23] L. B. Zhao, J. B. Delos, *Phys. Rev. A* **81**, 053418 (2010).
- [24] L. Wang, H. F. Yang, X. J. Liu, H. P. Liu, M. S. Zhan, J. B. Delos, *Phys. Rev. A* **82**, 022514 (2010).
- [25] D. H. Wang, S. H. Cheng, Z. H. Chen, *J. Electron. Spectrosc.* **202**, 62 (2015).
- [26] F. L. Liu, L. B. Zhao, *Phys. Rev. A* **95**, 043428 (2017).
- [27] N. Spellmeyer, D. Kleppner, M. R. Haggerty, V. Kondratovich, J. B. Delos, J. Gao, *Phys. Rev. Lett.* **79**, 1650 (1997).
- [28] M. R. Haggerty, J. B. Delos, *Phys. Rev. A* **61**, 053406 (2000).
- [29] Y. Q. Li, X. Y. Pan, V. Sahní, *J. Chem. Phys.* **139**, 114301 (2013).
- [30] D. H. Wang, Z. H. Chen, S. H. Cheng, *J. Phys. B* **49**, 205001 (2016).
- [31] C. Bracher, J. B. Delos, *Phys. Rev. Lett.* **96**, 100404 (2006).

*Corresponding author: lduwdh@163.com